Submitted to Rheologica Acta
October 4, 2012

High-flux Magnetorheology at Elevated Temperatures

M. Ocalan[1,2], G.H. McKinley[1]*

[1]*Hatsopoulos Microfluids Laboratory, Department of Mechanical Engineering, Massachusetts Institute of Technology, Cambridge, MA 02139, USA*

[2]*Schlumberger-Doll Research, Cambridge, MA 02139, USA*

Phone: 1-617-258-0754

Fax: 1-617-258-8559

* Corresponding author: gareth@mit.edu

Abstract

Commercial applications of magnetorheological (MR) fluids often require operation at elevated temperatures as a result of surrounding environmental conditions or intense localized viscous heating. Previous experimental investigations of thermal effects on MR fluids have reported significant reductions in the magnetorheological stress with increasing temperature, exceeding the predictions made by considering the thermal variations in the individual physical properties of the fluid and solid constituents of a typical MR fluid. In the low-flux regime, designers of MR fluid actuators can alleviate this thermal reduction in stress by increasing the applied magnetic field strength. However, because the fluid response to the applied field is limited in the high-flux regime by magnetic saturation, the ability to correct thermorheological changes are limited and it becomes necessary to explore and understand the intrinsic limitations of the fluid at elevated temperature. We describe a new magnetorheological fixture that is designed as a removable accessory to a commercial torsional shear rheometer. Careful consideration of the mechanical, thermal and electromagnetic design constraints enabled us to extend the operating range of the device. The assembled fixture is capable of applying magnetic flux densities up to 1T and controlling

the sample temperature up to 150°C. During the design of the instrument, close attention was given to the uniformity of the magnetic field applied to the sample by using finite element simulations. Incorporation of a custom-built magnetic flux sensor which matches the environmental capabilities of the fixture enables in-situ measurement of the local magnetic field at each temperature. The numerical results are also validated by spatially-resolved measurements of the local magnetic field throughout the sample. Finally, we explore the ability of a shift factor between fluid magnetization and yield strength to describe the measured variation in the MR fluid response at elevated temperatures.

Keywords: Magnetorheology, parallel-plate rheometry, finite element analysis, Mason number, power law scaling

1. Introduction

Magnetorheological (MR) fluids are suspensions of micron-sized magnetizable particles which undergo a large and reversible change in the rheological properties under an applied magnetic field (Rabinow, 1948, Klingenberg, 2001, de Vicente et al., 2011). The rheology and microstructure of MR fluids exhibit many similarities to those of electrorheological (ER) fluids (Bossis et al., 1997, Shkel and Klingenberg, 2001). In both types of fluids, an applied electromagnetic field generates interparticle interactions and leads to chaining and formation of column-like microstructures (Halsey and Toor, 1990, Fermigier and Gast, 1992, Promislow et al., 1995, Bossis et al., 1997, Tao, 2001, Climent et al., 2004, Deshmukh, 2007). In the absence of hydrodynamic forces caused by the flow of the suspending matrix, the chained microstructure is determined by the electromagnetic and contact forces. Bulk deformation and flow of the highly-anisotropic fluid is possible only when the percolated network of particle chains is broken. The material response is thus predominantly elastic up to a critical value of the imposed strain and a corresponding field-dependent critical stress or yield stress, $\tau_y(B)$ (Weiss et al., 1994, Li et al., 1999). Beyond this critical stress, the percolated structures are disrupted and the sample flows irreversibly as a viscoplastic material (Klingenberg and Zukoski, 1990). The Bingham plastic model has been widely used to describe the rheology of MR and ER fluids beyond the yield stress; however, more extensive measurements over a wider range of deformation rates show a progressive shear thinning nature of the post-yield properties and this leads to a better fit of experimental data by non-linear viscoplastic models such as the Casson or Herschel-Bulkley yield stress models (Gabriel and Laun, 2009).

MR fluid devices and actuators have been investigated for a number of applications such as automotive clutches, shock absorbing dampers, prosthetic knees and advanced

polishing applications (Jolly et al., 1998, Klingenberg, 2001, Kavlicoglu et al., 2006, Kordonski and Shorey, 2007). Recently, applications of MR fluids have also been investigated for oil & gas exploration and production (Cobern et al., 2007, Bhavsar et al., 2008). The subterranean operating temperatures for many oilfield applications can be relatively high (~150°C) because of the geothermal gradient. Furthermore, actuators are often operated in their high-field and high-force limit because of the constricted physical space available within the borehole. In a traditional industrial application, it may be possible to increase the dimensions of an actuator to achieve larger loads, however, the constraints on the size of the actuator in the downhole environment places a special emphasis on generating large fluid stresses. This means that MR fluids must be formulated to generate high shear stresses and operate under high flux densities. These stringent design requirements imposed by potential oilfield applications are the main motivators for the present study of the high-flux response of MR fluids at elevated temperatures.

Experimental measurements of the thermal dependence in magnetorheological effects

A number of previous experimental studies have explored the effects of temperature on MR fluids and devices at intermediate fields and for environmental conditions close to ambient temperature. These studies are summarized in Table 1. To provide a quantitative comparison between measured reductions in magnetorheological yield stress we define an average normalized sensitivity of the measured MR yield stress by:

$$\langle S_\tau \rangle = \frac{1}{\tau_y^0} \frac{\Delta \tau_y}{\Delta T}, \qquad (1)$$

where τ_y^0 is the yield stress at the reference temperature, T_0, and $\Delta \tau_y$ is the measured change in yield stress corresponding to a change in temperature, ΔT. Li and coworkers (2002) reported a reduction of magnetorheological yield stress in a commercial fluid (Lord® MRF-

132LD) corresponding to $\langle S_\tau \rangle = -2.2\times10^{-3} / °C$. Zschunke and coworkers (2005) studied the thermal sensitivity of another fluid (Lord® MRF-132AD), which is similar in composition to the previously mentioned fluid (Ponticel, 2002). When their data is fitted with a Bingham plastic model, the sensitivity of the yield stress is nearly threefold higher than that reported by Li and coworkers. Sahin and coworkers (2009) conducted experiments at elevated temperature on a magnetorheological grease formulated by suspending carbonyl iron particles in a commercially available grease and report a similar result of $\langle S_\tau \rangle = -3.7\times10^{-3} / °C$. Finally, Batterbee and Sims (2008) studied the effects of temperature on a commercial magnetorheological damper. The force response of the damper was characterized by a constitutive model including a yielding force that arises from the yield stress in the MR fluid. They observed a decreasing trend in this yield force with a temperature sensitivity in the same range as the mentioned rheological studies.

	Fluid / Device	B_{max} (T)	T_{min} / T_{max} $(°C)$	$\langle S_\tau \rangle$ $(10^4/°C)$
Li et al. (2002)	Lord® MRF-132LD	0.40	10 / 60	-22
Zschunke et al. (2005)	Lord® MRF-132AD	0.58	20 / 90	-73
Sahin et al. (2009)	Carbonyl iron in grease suspension	0.53	10 / 70	-37
Batterbee and Sims (2008)	Lord® RD-1005	-	15 / 75	-30

Table 1: Experimental studies of the thermal sensitivity of MR fluids. Here, B_{max} is the highest magnetic flux density at which the yield stress was evaluated. All studies reported significant reduction in the magnetorheological yield stress at elevated temperatures. To provide a quantitative comparison, the average normalized sensitivity $\langle S_\tau \rangle$ (See Equation 1 in text) is tabulated at the highest magnetic field studied in the respective study.

All of the referenced studies have identified significant and varying thermal sensitivity of the magnetorheological yield stress even within the moderate ranges of temperature increase explored ($T_{max} \leq 100°C$). In applications such as oil and gas production

that demand higher temperature operations than previously studied it is critical to be able to predict the extent of thermal reductions in the magnetorheological stress, so that appropriate design tolerances can be incorporated into devices.

Non-dimensional parameters for magnetorheology

For device design purposes, it is helpful to collapse rheological measurements over a range of field strength, temperature, shear rate and volume fraction into dimensionless master curves using suitable shift factors. This enables the device response to be predicted over a range of potential and future operating conditions. Suitable non-dimensional parameters specific to the flow of MR fluids can be determined by evaluating the different microscopic forces acting on the particles that comprise the aligned chained microstructure. An order of magnitude estimate of the magnetic force, $F_{mag} = (\pi/6)\mu_0 a^2 M_p{}^2$, can be obtained by using the uniform magnetization approximation for two spherical particles in contact (Klingenberg et al., 2007). Here μ_0 is the permeability of free space, a is the particle radius and M_p is the particle magnetization. The Reynolds number at the particle length scale is normally low and therefore a good estimate of the viscous force acting on a particle can be obtained from Stokes drag on a sphere, $F_d = 6\pi\eta_\infty a^2\dot{\gamma}$. Here η_∞ is the suspension viscosity in the high shear rate limit and $\dot{\gamma}$ is the imposed shear rate. The ratio of these two particle forces gives the Mason number:

$$Mn = \frac{\text{viscous force}}{\text{magnetic force}} = \frac{36\eta_\infty\dot{\gamma}}{\mu_0 M_p{}^2}. \qquad (2)$$

The suspension viscosity, $\eta_\infty(\phi)$, is used in the definition of *Mn* to account (in a mean field sense) for the increase in viscous drag on a single particle that is caused by the neighboring particles. At high volume fractions, MR suspensions may exhibit a small yield stress even in

the off-state due to jamming effects and therefore the measured viscosity $\eta(\dot{\gamma})$ of the suspension is also a function of shear rate. However, the viscosity is often found to plateau at high shear rates (Stickel and Powell, 2005) and this high-shear plateau value of the viscosity is commonly utilized in estimating the appropriate magnitude of viscous stress. If we assign representative numerical values to the quantities $\left(\dot{\gamma}_0 = 10s^{-1},\ M_p = 10^6 A/m,\ a = 2\times10^{-6} m,\ \eta_\infty = 0.2\ Pa.s\right)$ which are typical for a flow condition of interest in an oilfield application for MR fluids, we find $Mn \sim O\left(10^{-4}\right)$. Therefore, in terms of bulk rheology we expect the field-dependent yield stress to play a dominant role over the viscous stress that results from shearing flow.

Comparing the magnetic force to the characteristic Brownian force $k_B T/a$ acting on a particle gives another dimensionless parameter:

$$\lambda = \frac{\text{magnetic force}}{\text{Brownian force}} = \frac{\pi\mu_0 a^3 M_p^{\ 2}}{6k_B T}, \qquad (3)$$

where k_B is the Boltzmann constant and T is the temperature. Again substituting the typical characteristic values for $\mu_0,\ a,\ M_p$ and taking a characteristic temperature of $T \approx 450K$ we find $\lambda \sim O\left(10^9\right)$. It is clear that the magnetic forces in common flow situations of MR fluids dominate over Brownian forces even at the elevated temperatures that correspond to downhole conditions.

It is further possible to estimate the order of magnitude of the characteristic magnetic stress in the fluid by recognizing that the magnetic force acts on the surface of a unit cell that contains both the chained particle and the surrounding matrix fluid. For a uniform array of single columnar chains this corresponds, on average, to an area $A_p \approx \pi a^2/\phi$. Therefore, the expected magnetic stress scaling is:

$$\tau_{mag} \simeq \mu_0 \phi M_p^2 / 6 . \qquad (4)$$

This equation suggests a linear dependence of MR stress on volume fraction. Models based on particle chain mechanics, such as the one utilized to obtain this equation, lead to a prediction of linear dependence of stress on volume fraction (de Vicente et al., 2011). At lower values of volume fraction, this dependence has been demonstrated experimentally by Marshall and coworkers (1989), and also numerically by Klingenberg and coworkers (1991) for $\phi < 0.35$ in ER fluids. Felt and coworkers (1996) found a linear relationship in the range $0.014 < \phi < 0.12$ for an MR fluid. At higher values of ϕ the dependence is more complex, and the yield stress has been reported to demonstrate both a more rapid (de Vicente et al., 2011) or less rapid (Klingenberg et al., 1991) than linear increase with volume fraction.

Quite generally, we should thus expect the dimensionless yield stress exhibited by an MR fluid to be function of Mn, λ and the independent dimensionless volume fraction ϕ. Because $\lambda \gg 1$ for all temperatures of interest, any variation with λ can be neglected and the measured yield stress of the MR fluid scaled with the estimate of magnetic stress given by Equation (4) is only a function of Mn and ϕ, and may be expressed in dimensionless form:

$$\frac{\tau_y}{\tau_{mag}} = \Phi\left(Mn, \phi\right) . \qquad (5)$$

Theoretical predictions for changes in magnetorheology with temperature

All the microscopic forces considered in the functional relationship $\Phi\left(Mn, \phi\right)$ given in Equation (5) depend on physical quantities that evolve with the ambient operating temperature, T. The dependence of magnetic force on temperature arises from the effects of thermal fluctuations on ferromagnetic ordering within the particles. In the absence of an applied field, the ferromagnetic ordering is completely lost at the Curie temperature and the

material behavior becomes paramagnetic (Blundell, 2001). Below the Curie temperature, the saturation magnetization of the ferromagnetic material is a monotonically decreasing function of temperature (Jiles, 1991) and has been well characterized by experimental measurements. Measurements made on polycrystalline iron by Crangle and Goodman (1971) are shown in Figure 1 as an example. A functional form of the dependence of saturation magnetization on temperature, $M_S(T)$, can be obtained using a mean field approximation also known as the Weiss model of ferromagnetism, as illustrated in the figure. This model approximates the exchange interaction of neighboring atoms in a crystal by an effective field to solve for the ferromagnetic behavior of the material. This is not an accurate description of the interaction in metallic crystals because the ferromagnetism in these materials is largely caused by the conduction electrons; however, as shown in Figure 1, the Weiss model captures the general form of thermal response well across the complete range of temperatures. A detailed derivation of this and other models of magnetically-ordered condensed matter can be found in Blundell (2001).

Shul'man and coworkers (1980) studied the effects of temperature on a colloidal ferrofluid system near the Curie temperature. A strongly decreasing trend in the field dependent response near this critical temperature was demonstrated in their system ($T_C^{FF} = 145°C$). In contrast with the ferrofluid used in this earlier study, magnetorheological fluid particles are often composed of materials with very high Curie points (e.g., for iron, $T_C^{iron} = 770°C$). Thermal sensitivity is thus expected to be small. The slope of the saturation magnetization versus temperature curve that characterizes the thermal sensitivity becomes increasingly significant as the operating temperature approaches the Curie temperature. Using the measurements of Crangle and Goodman (1971), we can evaluate the sensitivity of the saturation magnetization of iron at 20°C:

$$S_M = \frac{1}{M_S^0}\frac{\partial M_S}{\partial T} = -1.1\times10^{-4}\ /\ ^\circ C\ . \qquad (6)$$

where M_S^0 is the saturation magnetization at the reference temperature. The magnitude increases only slightly at higher temperatures (e.g., $-1.7\times10^{-4}\ /\ ^\circ C$ at 130°C). Equation (4) suggests a quadratic dependence of the yield stress on saturation magnetization. Therefore, the sensitivity of the yield stress solely due to this effect is expected to be:

$$S_\tau^{\ M} \approx 2S_M = -2.2\times10^{-4}\ /\ ^\circ C\ . \qquad (7)$$

Compared to the previous measurements of yield stress at elevated temperatures (Table 1), the change in magnetization contribution is at least an order of magnitude less than the actual measured thermal reduction in the bulk yield stress.

The Brownian force acting on the suspension particles also becomes higher as the background temperature is increased (Li et al., 2002); however, as seen by the large numerical value of λ, the magnetic force completely dominates over Brownian forces at all temperatures. For example, the increase in the Brownian force resulting from a temperature rise from 25°C to 770°C (i.e. the Curie temperature of iron) only corresponds to a factor of three change in λ. Therefore, dimensional analysis suggests that the effects of thermal fluctuations on the particle structures in an MR fluid should have a negligible effect on the tendency for particle chaining and the resulting magnetorheological yield stress.

The suspension viscosity in the absence of an external magnetic field is also a strong function of temperature. This is largely due to the change in the matrix fluid viscosity, which typically varies according to the Arrhenius relationship (Bird et al., 1987):

$$\eta_\infty(T) = \eta_\infty(T_0)\, e^{\frac{\Delta H}{R}\left(\frac{1}{T}-\frac{1}{T_0}\right)}, \qquad (8)$$

where T_0 is the reference temperature, ΔH is the activation energy for flow and R is the universal gas constant. From dimensional considerations we have argued that the suspension

viscosity appears only in the expression for viscous drag on particle chains and is therefore only present under flowing conditions. Therefore, the static yield stress that dominates the MR response should not be affected by the changes in the matrix fluid viscosity.

It thus remains unclear as to what particular physical mechanism leads to the large values of the thermally-induced changes in the MR yield stress that have been previously reported. For accurate design of downhole devices we need to document these changes and therefore pursue direct experimentation under appropriate thermal and magnetic conditions.

High-flux magnetorheometry

Bulk rheological characterization of MR fluids is conducted by the simultaneous application of magnetic fields and shearing strain fields to the fluid samples in a rheometer. The magnitude of the MR response observed depends on the relative orientations of these two vector fields (Kuzhir et al., 2003a, Kuzhir et al., 2003b, Kuzhir et al., 2009). The vast majority of experimental instrumentation generates magnetic fields that are aligned in the perpendicular direction to both the flow streamlines and the vorticity (de Vicente et al., 2011), primarily because this field orientation occurs in most MR fluid devices (e.g., dampers, clutches). In Table 2, we survey published reports of rheometers and rheometer accessories that have been built to investigate MR fluid rheology in the intermediate and high applied field ranges. Torsional shearing rheometers have been utilized most often in these studies because of the ease of loading the MR fluid sample and the ability to construct a custom magnetorheology accessory that can be fitted to a commercial instrument, utilizing instrument grade sensors and control systems. The development of capillary magnetorheometers has mainly been motivated by the need for rheological investigations at high shear rates. Because of the high rates of viscous dissipation that occur in such devices (at high stresses and high deformation rates), exploring this regime using a small sample of

fluid in a rheometer with closed streamlines poses challenges in heat removal. The continuous convective removal of heat from a capillary rheometer has been shown to be an effective solution to this problem. It should also be noted that, none of the devices with high-flux capability ($B_{\max} \sim O(1T)$) have been used to investigate the magnetorheological response at high temperatures ($T_{\max} \geq 100°C$).

Table 2: A survey of custom-designed high-flux magnetorheology accessories, associated rheometers and the maximum accessible magnetic flux density, $B_{\max}$. Many studies utilize a magnetorheology accessory mounted on a commercial torsional shearing (CTS) rheometer, taking advantage of the high dynamic range sensors and actuators of these instruments.

Reference	Geometry and rheometer	$B_{\max}(T)$
Laun et al. (1996)	Double concentric cylinder, CTS	0.4
	Custom designed capillary rheometer	0.4
Rankin et al. (1999)	Parallel plate, CTS	0.4
Park et al. (2001)	Parallel plate, CTS	0.33
Horvath et al. (2002)	Parallel plate, CTS	2.0
Genc and Phule (2002)	Double concentric cylinder, custom designed	0.78
Deshmukh and McKinley (2004)	Parallel plate, CTS	0.64
Laeuger et al. (2005)	Anton Paar® MRD-1T device, CTS	1.0
Ulicny et al. (2005)	Concentric cylinder, custom design	~1T
Wang and Gordaninejad (2006)	Custom designed capillary	0.35
Gabriel and Laun (2009)	Custom designed capillary	0.3
Laun et al. (2010)	Twin gap parallel plate, CTS	1.5

In this survey, we have identified two outstanding open issues in experimental magnetorheology. Firstly, we have shown that the theoretical predictions for the thermal sensitivity of the change in yield stress expected at high temperatures are an order of magnitude smaller than the measured values reported in literature. Secondly, high-flux magnetorheology has not been investigated under elevated temperatures. In the present work, we study a larger range of temperatures and magnetic fields than those that have been investigated to date as summarized in Tables 1&2. To explore high-flux and high-

temperature conditions simultaneously, a new magnetorheology fixture is designed and built to work in conjunction with a commercial torsional shear rheometer. In Section 2, we outline specific mechanical, magnetic and thermal design aspects of the instrumentation. In Section 3, experimental results obtained with the new fixture are presented. In addition, the evolution of the yield stress measurements with the increasing field strength is used to evaluate the predictions of previously-identified power law scalings. In Section 4, our findings are summarized and the conclusions are presented.

2. Instrument Design

2.1. Mechanical integration and material selection

The magnetorheometry fixture is designed to work with the TA Instruments® AR-G2™ stress-controlled rheometer and is centralized to the rheometer spindle axis by means of complementary mating mechanical features that align with the rheometer base casting. The sample space within this fixture is compatible with a $20mm$ parallel plate geometry with a maximum sample thickness, $h = 0.5mm$. General construction features of the new MR fixture are illustrated with a schematic diagram and a photograph in Figure 2.

The fixture generates a magnetic field in the sample by the use of a toroidal electromagnetic coil. The magnetic field is channeled primarily through a series of magnetically-permeable components. Often referred to as a magnetic circuit, these components are used to minimize the required electrical power input and to focus the field as uniformly as possible through the MR fluid sample. The MR fluid sample is located in a narrow gap between two magnetically-permeable components near the center of the fixture. These components are manufactured out of 1018 carbon steel for its high relative

permeability (μ_r) and low coercivity (H_c) properties. These magnetic properties are highly dependent on processing, heat treating and machining; and were not measured for the specific material used. For reference, they have been reported for 1010 carbon steel, a similar grade of material, to be $\mu_{r,1010CS} = 3800$ and $H_{c,1010CS} = 80 - 160 A/m$ (Stedfeld and Zorc, 1995). Utilizing a low-coercivity material is advantageous since this minimizes the remnant field that is retained within the fixture upon removal of the magnetic field.

Components that are not a part of the magnetic circuit often need to have a low magnetic permeability so that the leakage field is minimized. Contrary to conduction or heat transfer problems where highly insulating materials can be selected to isolate the flux of electric current and heat, respectively, the range of available material properties does not allow the designer to vary magnetic permeability within power magnetic circuits much beyond a factor of $\sim 10^2$ at high fields. Although diamagnetic materials are less permeable than free space (e.g., relative permeability of bismuth, $\mu_{r,Bi} = 0.9999834$ (Serway, 1990)), this effect is often negligible when compared to ferromagnetism (e.g., steel $\mu_{r,steel} \approx 1000$). The same can be said about common paramagnetic materials such as aluminum ($\mu_{r,Al} = 1.000023$ (Serway, 1990)). Therefore, in the analysis and design of static magnetic field generators and actuators, non-ferromagnetic materials can be freely used near a magnetic circuit with little regard to their specific magnetic characteristics. Consequently, we selected aluminum for the non-magnetic spacer, the bobbin for the coil winding and for the channel plate that houses the upper spiral flow channels (discussed in detail below). The upper plate geometry was manufactured using a titanium alloy. Utilizing a magnetic material in the upper plate geometry is advantageous in better focusing of the field and reducing particle slip (Laun et al., 2011, Ocalan and McKinley, 2012). The latter benefit arises because of the attractive magnetic forces between the plate and the suspended MR particles. However,

a magnetic upper plate placed within the applied field will experience a magnetic body force in both the axial and transverse directions. Design estimates suggest that at large fields ($B \sim 1T$) these forces are significantly larger than the normal load capabilities of the thrust bearings of commercial rheometers. Because of these concerns, a non-magnetic material is selected for the upper plate.

Electrical conductivity is also an important property that affects material selection in electromagnetic design. However, the operation of the magnetorheology fixture is often in a regime where the effects of conductivity are negligible. Under transient magnetic fields, an electric field is generated within a material element according to Faraday's Law, which in turn induces currents depending on the electrical conductivity of the material. If large enough, these induced currents may affect the magnetic field and the magnetorheological measurements. This can be quantified by the magnetic diffusion time constant, $\tau_m = \mu\sigma d^2/\pi^2$ (Woodson and Melcher, 1968), where σ is the electrical conductivity and d is the length scale of interest. In the magnetorheology fixture, with $d \sim 0.01m$ and $\sigma \sim 10^7\ S/m$ (Avallone and Baumeister III, 1996), this time scale is in the order of $100ms$ which is much smaller than the stabilization periods allowed for the rheological measurements in this study.

It is also possible to generate a time-varying magnetic field on a material element by advecting it through a spatially-varying magnetic field. Although the titanium upper plate of the fixture is rotating within a magnetic field, in a perfectly aligned system, there would be no magnetic field transients cased by this rotation due to the axisymmetry of the field. Therefore, the conductivity of the upper plate is not an important quantity to control in the design of the instrument. This analysis of the time scale for magnetic diffusion and the conclusions on the effects of time-varying magnetic fields are in agreement with the experimental findings of Laun and Gabriel (2007). Furthermore, all experimental work presented herein, have been

conducted in conjunction with measurements of the steady magnetic field to ensure that transient induced fields have no measurable effect on the results.

In a solenoidal electromagnetic coil, such as the one used in the present magnetorheology fixture, the maximum alignment of the field lines is commonly achieved near the axial midpoint of the solenoidal coil. Therefore, it is desirable to design the sample location to be near this point. However, the presence of a coil around the sample geometry would cause difficulties in loading and trimming the MR fluid sample. For this reason, the physical location of the windings is designed to be completely below the sample plane whereas the magnetic core is continued above the sample through the custom design of the top covers that are machined from carbon steel to help close the magnetic circuit.

The large currents present in the windings during application of the magnetic field mean that there is considerable resistive heating $(\sim 200W)$ that takes place within the fixture. If it is not dissipated effectively, this heating may raise the temperature of the fluid sample and possibly cause the components of the MR fixture to overheat. For these reasons, we have included fluid circulation channels within the fixture. The flow path consists of two spirally cut channels (Figure 3) on each side of the electromagnetic coil that are linked with an annular flow section past the winding. On each end of the channel a quick-connect pressure fitting is provided and all component interfaces have been sealed with o-rings. During operation at elevated temperatures the temperature of the circulation fluid can be as high as 150°C. Furthermore, because of resistive heating and thermal diffusion, other locations in the fixture may reach locally higher temperatures. To enable safe and stable experiments at this operating point, fluorocarbon o-ring seals, polyimide-coated magnet wire and fluorinated ethylene propylene lead wires were used. Details of the thermal design are presented in Section 2.3 below.

To accurately measure the true rheological properties of the MR fluid, wall slip in the rheometer geometry needs to be avoided (Barnes, 1995, Bertola et al., 2003). This is especially important for the magnetorheology fixture as the strong particle-particle magnetic interactions, which lead to the bulk MR response, are not present between the non-magnetic plates and the first layer of adjacent particles. In the experiments we use roughened fixture surfaces to enhance the interaction between the walls of the geometry and the MR fluid particles. The non-magnetic spacer forming the lower plate was roughened by a sandblasting operation to a surface roughness of 3.83 microns (rms) and the upper plate was used with 600-grit adhesive-backed sandpaper (average particle size $20\mu m$) adhered to its surface. This method eliminated slip in static yield stress measurements and was verified by independent creep tests over a range of applied stresses.

As a result of the discontinuity of magnetic permeability at the radial perimeter of the sample, an outward magnetic body force on the MR fluid is generated. This radial body force is resisted only by the surface tension of the fluid sample. When the applied magnetic field is large enough, the magnetized material can be ejected out of the geometry. Similar effects have been observed previously (Deshmukh, 2007, Laun et al., 2008a). In our experiments, sample integrity was ensured by using an elastomeric ring with a rectangular cross-section stretched around the top geometry, as illustrated in Figure 2. A method for estimating the critical field that results in sample escape is presented in the Appendix.

2.2 Magnetic Design

The present magnetorheology fixture can generate a magnetic flux density through the sample of up to $B \approx 1T$. The main goal of the magnetic design of the instrument was to generate this level of field within the size restrictions placed by the geometry of the

rheometer with minimal spatial variation in the flux density, $\mathbf{B}(r,z)$. Design analysis was conducted primarily using finite element methods. Approximate analytical relations were used in preliminary sizing of components through application of integral forms of Ampere's Law and Gauss' Law. These relations can be found in many electromechanical references and literature (Avallone and Baumeister III, 1996, Laun et al., 1996). Because of the complex geometry of the magnetorheology fixture and the non-linear response of the material (which are not incorporated in the approximate analytic relations) numerical simulation is essential to accurately predict the actual magnetic field that is realized in the new MR fixture.

Since the magnetic flux density is divergenceless ($\nabla.\mathbf{B}=0$) a magnetic vector potential can be defined such that, $\mathbf{B}=\nabla\times\mathbf{A}$ and $\nabla.\mathbf{A}=0$. The second equation, which is called the Coulomb gage (Jackson, 1999), is required since defining only the curl does not uniquely identify the vector field $\mathbf{A}$. Substituting these equations into the differential form of Ampere's Law results in a vector Poisson equation in three space coordinates ($\nabla^2\mathbf{A}=-\mu\mathbf{J}$). By invoking the axisymmetry condition, the problem is reduced to a one dimensional form ($\left[\nabla^2\mathbf{A}\right]_\theta=-\mu J_\theta$) for the magnetorheometry fixture where,

$$\mathbf{B}=-\frac{\partial A_\theta}{\partial z}\mathbf{i}_r+\frac{1}{r}\frac{\partial}{\partial r}\left(rA_\theta\right)\mathbf{i}_z. \qquad (9)$$

The general formulation for analytical boundary value problems is described in many electromagnetic texts (e.g., Zahn (1987)). The specifics of the numerical formulation and solution methods are discussed in more detail in dedicated texts (see for example Ida and Bastos (1997)).

The numerical analysis was conducted with Maxwell® 2D software developed by Ansoft Corporation®. The magnetorheometry fixture was modeled using an axisymmetric formulation and design iterations were made to size components and to minimize leakage and saturation of the magnetic circuit components. After determining the feasibility of generating

1*T* flux density through the sample, within the space constraints posed by the rheometer, the radial variation of magnetic field in this region was minimized using heuristic iterative methods. Because of the specific geometrical features in the vicinity of the central spindle axis and near the radial edge of the sample, the magnetic field uniformity deteriorates in these two regions.

The source for field non-uniformity near the sample axis is the rheometer spindle access hole in the portion of the magnetic circuit that is above the sample. This undesirable variation in magnetic field is difficult to correct for because of the non-linear response of MR fluids to applied field. The variation can be minimized by limiting the diameter of the shaft and the size of the access hole, however this comes at the cost of introducing additional torsional compliance to the rotating spindle. To minimize this added torsional compliance, a notched spindle with varying diameter was designed, as shown in Figure 2. The notch on the rheometer spindle has rounded edges in order to minimize stress concentration and sits in a complementary hole geometry with a minimum diameter of 7.3 mm. The improvement to the magnetic field uniformity is presented in contour and line plots in Figure 4.

The compliance of the rheometer spindle will either have no impact on the measurement (e.g., after steady-state is achieved in steady shear experiments) or can be easily corrected for by a linear constitutive relation. In commercial rheometers, including the AR-G2™, the compliance in the spindle is corrected for by built-in calibrations and software functions. One limitation to this correction arises in the case of a torsional compliance that is so high that additional spindle dynamics are introduced within the working frequency range of oscillatory experiments. This behavior can be estimated by a lumped parameter simple oscillator model in which the stiffness element is equal to the reciprocal of the torsional compliance and the mass element equal to the moment of inertia of the test geometry below the notch. In this analysis, additional viscous damping provided by the sample can be ignored

to achieve a conservative estimate, as any additional damping would be favorable to the analysis. The undamped resonant frequency for the notched rheometer fixture is estimated to be 6.4 kHz, which is well above the rheometric frequency range of interest. An experimental validation of this analysis was conducted in which a sinusoidal torque was applied to the geometry with constant amplitude and frequency sweep up to 100Hz (maximum operating frequency for the AR-G2™ rheometer). No additional dynamical effects were observed.

It can be seen from the plots of $B(r,z)$ in Figure 4 that there is a significant variation of the magnetic field near the perimeter of the magnetic core; this is caused by the discontinuity of magnetic permeability in this region. Using a sample geometry that is smaller in diameter than the magnetic core is not a valid approach because the magnetic permeability of the sample itself leads to a significant field variation near its own perimeter. Contour and line plots of magnetic flux density of a 12mm diameter sample of Lord® MRF-132DG fluid in the magnetorheology fixture are presented in Figure 5a to illustrate this effect. The fluid properties in this model calculation includes the full non-linear magnetization curve of the MR fluid (Lord, 2008). It can be seen from Figure 5 that there is a large increase in the magnetic field near the sample perimeter. Inspection of the flux lines near the perimeter indicate that the cause of the non-uniformity is the discontinuity of permeability, focusing more of the local magnetic field through the sample. Matching the sample diameter with the magnetic core amplifies this non-uniformity even more as illustrated in Figure 5b.

A method of reducing the magnetic field non-uniformity near the sample perimeter is to place the sample axially near the center of the air gap by the use of a non-magnetic spacer, as illustrated in Figure 5c. In this case, the magnetic field is still focused around the perimeter, however, spatially this also corresponds to an area where the magnetic field is de-focusing and spreading radially outward. These two effects counteract each other and the non-uniformity near the sample perimeter is reduced. A similar conclusion has been

previously reached in the study by Laun and coworkers (2008b); by analyzing the field variations in a commercial magnetorheology accessory these researchers recommended a straightforward modification to the design features of the magnetic circuit.

Spatially-resolved measurements of the magnetic field were taken to evaluate the accuracy of the finite element model computations. An F.W. Bell® 5180 gaussmeter (with a circular sensing region of diameter $0.381mm$) was used in a groove designed within the non-magnetic spacer. The magnetic flux density obtained by the finite element models and the measurements show good agreement (Figure 6). In contrast with the previous plots shown in Figures 4 & 5 that presented magnetic flux density within the MR fluid sample, the curves shown in Figure 6 are for the magnetic flux density $B(r)$ at the sensor location. Another important feature to note in the radial variation of magnetic field is that the field is nearly uniform near the mid-span radius $(r_{ms} = 0.5R)$ of the sample geometry, and attains an almost constant plateau value for $0.4 \le r/R \le 0.7$ where $R = 10mm$ is the radius of the upper plate.

The Hall effect probe of the gaussmeter cannot be operated at the elevated temperatures $(T \sim 150°C)$ targeted in this study. To provide a measurement of magnetic field at temperatures above 70°C, a custom secondary coil, pictured in Figure 7, was manufactured. The total number of windings was $N = 100$, with 50 turns in each direction. This type of winding configuration provides maximum sensitivity to the magnetic field at the midspan radius, r_{ms} but no sensitivity to magnetic field in radial positions below minimum radius, $r_{\min} = 3.2mm$ $(r_{\min}/R = 0.32)$, or above the maximum radius, $r_{\max} = 8.0mm$ $(r_{\min}/R = 0.8)$. Therefore the high sensitivity region of the secondary coil corresponds with the magnetic flux plateau in the sample chamber. The time integration of Faraday's Law gives the relation between the voltage across the coil and a series of spatial integrals of the magnetic field:

$$\int_0^{t^*} V dt = \sum_{CW} \int_S B_z dS - \sum_{CCW} \int_S B_z dS = K_W B_z . \qquad (10)$$

Distinction between the clockwise (CW) and counterclockwise (CCW) directions (as viewed in the +*z* direction) is made since their contributions to the measured voltage are in opposite polarity with respect to each other. With the knowledge of the spatial distribution of magnetic field and windings, or by making simplifying approximations, the coefficient of proportionality K_W between the axial magnetic field and the time integral of the measured voltage may be found. In the magnetorheometer setup the secondary coil was connected to an integrating fluxmeter (Lakeshore® Model 480™). The measurement output of the fluxmeter, i.e. the time integral of voltage, was calibrated experimentally with the Hall effect probe measurements to determine $K_W = 2.16 \times 10^{-3} VsT^{-1}$.

2.3 Thermal Design

The magnetorheometry fixture is designed for sample temperatures up to 150°C. At this temperature the resistive heating can result in dissipation of up to 200W in the electromagnetic coil. The two main goals in the thermal design of the instrument are: 1) to control sample temperature and 2) to remove heat away from the electromagnetic coil efficiently such that the change in sample temperature due to resistive heating is minimal. This was accomplished by fluid circulation within the fixture. The fluid circulation path, illustrated in Figure 3, is made up of two spiral grooves on the plates mating with each of the coil bobbin walls, which are interconnected by an annular flow channel between the magnetic core and the bobbin.

The majority of the resistive heat generated in the electromagnetic windings is carried away from the fixture by conduction across the coil windings and the bobbin and then, in turn, by convection to the circulation fluid. For use in the numerical calculations of this heat

transfer problem, the effective thermal conductivity of the windings was estimated using a correlation (Agarwal et al., 2006) employed for long-fiber unidirectional composite laminates of high conductivity fibers embedded in a low conductivity matrix:

$$k_{eff} = k_{ins}\frac{1+\phi_c}{1-\phi_c}, \qquad (11)$$

where k_{ins} is the thermal conductivity of the electrical insulation, and ϕ_c is the conductor volume fraction in the electromagnetic coil. This correlation is only valid in the directions orthogonal to the fibers (i.e. in the radial and axial directions in our geometry); however, as a result of the axisymmetry, these are the only relevant directions in this heat transfer problem. Convective heat transfer coefficients in each flow channel were calculated by utilizing well-known relations for pressure-driven flow, provided in many heat transfer texts such as that of Mills (1999).

To determine the rate-limiting heat transfer process, the Biot number, $Bi = h_c\left(H/2\right)/k_{eff}$ can be used. Here, $h_c \approx 3000 Wm^{-2}K^{-1}$ is the convective heat transfer coefficient, which is found as a function of the Reynolds number and Prandtl number in the circulating fluid, and *H* is the height of the coil. This dimensionless parameter is found to be approximately $Bi = 45$ for this device, which indicates that conduction is the slower heat transfer mechanism. To estimate the maximum coil temperature resulting from the resistive heating process a numerical model of heat transfer was generated using Quickfield™ (Tera Analysis Ltd.). This problem has analogies to the axisymmetric magnetostatic problem described in the previous section. In the heat transfer case, Poisson's equation is $\nabla^2 T = -q'''/k$, where q''' is the rate of volumetric heat generation and k is the thermal conductivity. The top, bottom and inner surface boundary conditions correspond to convective boundaries and the outside surface is a no flux condition. Because of the thermal

insulation this last condition is a conservative approximation to the weak natural convection present on this vertical cylindrical surface ($h_c \approx 5 W m^{-2} K^{-1}$).

For comparison with numerical results, an approximate analytical solution was also calculated. Neglecting convective heat transfer in the annular flow channel and the conductive resistance posed by the bobbin, the temperature field $T(z)$ of the coil is found to be:

$$T(z) = T_f + \frac{QH}{\pi k_{eff}\left(r_o^{\,2} - r_i^{\,2}\right)}\left(\frac{1}{Bi} + \frac{z}{2H} - \frac{z^2}{2H^2}\right), \qquad (12)$$

where T_f is the circulation fluid temperature, Q is the total rate of resistive heat generation, and r_i and r_o are the inner and outer radii of the windings.

The results of the analysis are presented in Figure 8 as a contour plot of the numerical analysis and a line plot comparing the maximum axial variations of temperature obtained by the analytical (1D) and numerical (2D) methods. There is good agreement between the models, however the 1D solution slightly overestimates the maximum temperature in the center of the winding and the bobbin because heat rejection to the inner surface in this model is neglected.

To evaluate the capability of the instrument to remove the resistive heat that is generated in the windings, an experiment was conducted in which cooling fluid was continuously circulated and a step in current of $I = 5A$ was applied to the instrument while monitoring the sample chamber temperature and coil resistance. The change in the coil resistance ΔR can be related to the average temperature of the coil

$$T_{av} = T_0 + \frac{1}{\alpha_{Cu}}\frac{\Delta R}{R_0}, \qquad (13)$$

where $\alpha_{Cu} = 0.00393 K^{-1}$ is the temperature coefficient of resistivity, and T_0 and R_0 are the initial temperature and coil resistance, respectively (Avallone and Baumeister III, 1996,

Sect.15-1). This measurement is a desirable alternative to inserting temperature sensors in the coil and risking breaking the insulation integrity during the installation and removal. Evolutions of average coil temperature and sample chamber temperature are presented in Figure 9. The temperature rise of the bottom plate of the geometry is only 4°C even at a current of $I = 5A$ corresponding to a magnetic flux density $B = 1.0T$.

3. Experimental Results

To evaluate the MR fluid response to the imposed magnetic field, a series of shear-rate-controlled experiments were conducted on a commercial MR fluid (MRF-132DG fluid manufactured by Lord Corporation®). To ensure repeatability in the measurements a test protocol developed by Deshmukh (2007) was followed. Prior to the experiments the fluid samples were mixed for more than 8 hours on a benchtop roller mixer (Wheaton®, Model 348921UL) at approximately 10rpm. After the fluid sample was loaded in the rheometer, a field in excess of 0.5T was applied for more than 30 seconds. This step was utilized in order to allow the fluid to form stable structures within the sample chamber. The field was removed and the sample then was pre-sheared at $\dot{\gamma}_{ps} = 300s^{-1}$ for more than 60 seconds to disrupt any residual chained structures. Following this step, the measured fluid rheology was found to be independent of loading history. The repeatability of experimental measurements in previous work (Deshmukh, 2007) and the present study strongly supports this assertion .

3.1 Measurements at ambient conditions

The steady shear measurements are presented in Figure 10. The magnetic flux density reported is the plateau value measured at a mid-span radius of $r_{ms} = 5mm$ by using the gaussmeter probe (for ambient temperature experiments) and the calibrated secondary coil

(for experiments at elevated temperatures). The local shear rate in the parallel plate geometry is zero on the symmetry axis of the geometry $(r = 0)$ and linearly increases to its maximum value, $\dot{\gamma}_R$, at the geometry rim assuming there is no slip on the roughened fixtures. The reported shear stress values account for the non-uniform shear rate in the sample with a Rabinowitsch type correction (Macosko, 1994):

$$\tau = \frac{\mathcal{T}}{2\pi R^3}\left[3 + \frac{d\ln\mathcal{T}}{d\ln\dot{\gamma}_R}\right], \qquad (14)$$

where $\mathcal{T}$ is the measured torque on the rheometer spindle and R is the plate radius. The logarithmic derivative in this equation is unity for Newtonian fluids and zero for perfectly shear thinning fluids $(\eta = \tau_y/\dot{\gamma})$. For MR fluids this term is normally much closer to the latter case; however, in order to increase the accuracy of the measurements, this correction was utilized by fitting a fifth-order polynomial to the $\ln\mathcal{T}$ vs. $\ln\dot{\gamma}_R$ raw data, and in turn each data point was corrected according to the logarithmic derivative calculated from this polynomial function (Ewoldt et al., 2010). The rate-dependent viscosity is reported at the rim shear rate and calculated using the expression:

$$\eta_R = \frac{\tau}{\dot{\gamma}_R}. \qquad (15)$$

In the plots of shear stress vs. shear rate (Figure 10(a)), the dominant role of the yield stress in the rheology of MR fluids is evident. These plots remain essentially flat over four orders of magnitude in shear rate. Plots of the viscosity variation with decreasing shear stress (Figure 10(b)) show that at all field levels the viscosity diverges towards infinity while the stress approaches an asymptotic value. We determine the dynamic yield stress as this asymptotic value. In the field-off state the fluid also has a weak yield stress as expected for a high volume fraction suspension (the fluid is 32% v/v). However, when compared to the field-on yield stress, this value is exceedingly small.

It is important to understand the evolution of the MR yield stress with applied field for design purposes. Plots showing the evolution in the yield stress with variations in the magnetic field strength, H and magnetization, M are presented in Figure 11. At low fields both of these variations follow the scaling laws previously described by Ginder and coworkers (1996) in the case of field strength, and Klingenberg and coworkers (2007) for magnetization. However, in the high field regime the variation deviates significantly from these scaling laws. This deviation from the simple scaling law ($\tau_y \sim H^{3/2}$) is expected since this power law relation is applicable only in an intermediate field regime, in which the magnetic interactions in the suspension are significantly affected by the magnetic saturation of the contact points between the particles (Ginder et al., 1996). In comparison with the predictions of this $3/2$ power law, the scaling of Klingenberg and coworkers ($\tau_y \sim M^2$) better match the measurements across the broad range of magnetic field applied; however, the measured dependence of the yield stress shows a sub-quadratic scaling at higher field levels (corresponding to $B > 0.3T$).

3.2 Magnetorheological stress at elevated temperatures

The effect of temperature on magnetorheological response is evaluated for three levels of magnetic flux density and presented in Figure 12. Measurements on five samples were taken at three temperatures each: $T = 20$, 75 and 130°C. At the highest two temperatures, the flux density was measured with the secondary coil and integrating fluxmeter. At 0.3T, the current necessary to generate this field was the same at all temperature levels tested. However, at higher flux densities, the current requirement was found to be higher at elevated temperatures (leading to a magnetic field correction of up to approximately 5%). This is attributed to the thermomagnetic properties of the magnetic material used in the magnetorheometer fixture. Therefore, making measurements at elevated temperature without

a calibrated magnetic field sensor in place may introduce an undesirable device-specific systematic error into the measurements.

The high-temperature results show a systematic and statistically significant decline in magnetorheological stress with increasing temperature. In Section 1, an average sensitivity parameter, $\langle S_\tau \rangle$, was defined to compare quantitatively the changes observed by different studies of magnetorheology in the literature and the changes predicted by theory. The experimentally-determined values for this sensitivity parameter and the dynamic yield stress obtained from our high temperature measurements are tabulated in Table 3. When compared to values reported previously, the thermal sensitivities measured in the present study are lower, and closer to the values obtained by theoretical estimates discussed in Section 1.

$B(T)$	$\tau_y^D\,(kPa)$			$\langle S_\tau \rangle\,(10^4/°C)$	
	$20°C$	$75°C$	$130°C$	$20°C \rightarrow 75°C$	$75°C \rightarrow 130°C$
0.3	10.8	10.2	9.9	-10.1	-5.3
0.6	28.5	27.0	25.8	-9.6	-8.1
0.9	41.6	39.3	37.2	-10.1	-9.7

Table 3: Evolution of magnetorheological yield stress with temperature and magnetic field. The dynamic yield stress, τ_y^D, is measured as the asymptotic value in the fluid stress as the shear rate is reduced towards zero. The average normalized sensitivity parameter, $\langle S_\tau \rangle$, is reported for comparison with the values in Section 1 in terms of an average value between 20°C to 75°C and 75°C to 130°C.

The dependence of MR stress on applied field and temperature is a non-trivial function of a number of parameters (as discussed in Section 1); however, by evaluating these dependencies separately and applying appropriate shift factors to the measurements, we can construct a rheological master curve from the data presented above. We define individual shift factors that capture changes in the yield stress associated with changes in temperature (a_Y) and magnetization (a_M) and a resulting reduced stress

$$\tau_r = \frac{\tau(M,T,\dot{\gamma})}{a_M a_Y}. \qquad (16)$$

The shift in the yield stress associated with the changes in temperature from a reference condition τ_y^0 at the reference temperature T_0 (here taken to be $T_0 = 20°C$) can be calculated from the experimental data by a yield stress shift factor that is related to the thermal sensitivity defined in Section 1:

$$a_Y = 1 + \langle S_\tau \rangle \Delta T. \qquad (17)$$

We next consider changes in the yield stress associated with changes in the applied magnetic field. As we see from the plot in Figure 11, at high fields this dependence does not follow the scaling laws previously described in the literature. For this reason we take a more general functional relationship for the magnetization shift factor

$$a_M = \left(\frac{M}{M_0}\right)^\alpha, \qquad (18)$$

where α is an empirically-determined exponent and M_0 is an arbitrary reference magnetization. In the present study this parameter is taken to be the MR fluid magnetization corresponding to the value at a magnetic flux density of $B = 0.3T$, which is $M_0 = 1.96 \times 10^5\ A/m$ (as published by the manufacturer of the fluid (Lord, 2008)).

As discussed in Section 1, we expect the reduced stress τ_r to be a function of an appropriately defined reduced shear rate (or in dimensionless form the Mason number Mn). Since the Mason number is a dimensionless ratio of the viscous stress to the magnetic stress and we have already defined how the latter quantity is shifted (Equation(16)), we only need to define a thermoviscous shift factor

$$a_T = \frac{\eta_\infty(T)}{\eta_\infty(T_0)} = \exp\left[\frac{\Delta H}{R}\left(\frac{1}{T} - \frac{1}{T_0}\right)\right], \qquad (19)$$

to account for the change in the viscosity of the base fluid. The second equality in Equation (19) is obtained by making use of Equation (8).

The resulting master curve for this MR fluid evaluated from these three distinct physical mechanisms is presented in Figure 13. The shifted vertical axis is the reduced stress $\tau_r = \tau/(a_M a_Y)$ and the horizontal axis is the reduced shear rate $\dot{\gamma}_r = \dot{\gamma}_R a_T/(a_M a_Y)$. The data superposes well, demonstrating that each of the different physical mechanisms contributing to the measured changes in MR fluid rheology can be well captured by the individual magnetic and thermal shift factors. The master curve is essentially flat with the reduce stress equivalent to the reference yield stress $(\tau_r = \tau_y^0)$ corresponding to the reference temperature T_0 and reference magnetization M_0. The empirically determined power law index is found to be $\alpha = 1.46 \pm 0.07$ within 95% confidence bounds. This value indicates a clear sub-quadratic scaling of the MR stress τ_y with magnetization M.

4. Discussion and Conclusions

A new high-temperature and high-flux magnetorheometry fixture was designed to be used with a commercial torsional shear flow rheometer. Using finite element methods, the magnetic field uniformity in the sample chamber was evaluated and improved by implementing a number of design features to the new MR fixture. The numerical results were verified with spatially-resolved measurements of the local magnetic field across the parallel plate geometry used to contain the test fluid. The design of the fixture also allows for in-situ radially-resolved magnetic field measurements while the sample is under test. During rheological measurements under ambient temperature conditions, a commercial Hall effect probe is used for such measurements. For high-temperature measurements, a custom-wound and calibrated secondary coil was used in conjunction with an integrating fluxmeter. The key

thermal features of the new fixture design include oil circulation flow channels for sample temperature control. This thermal management system was shown to be effective in regulating both the sample and bobbin temperature.

The fixture was used to evaluate the variation in the MR stress with shear rate and magnetic field at ambient and elevated temperatures. Comparison of the experimental results shows a systematic reduction in the magnetorheological yield stress with increasing temperature. A yield stress sensitivity parameter a_Y was defined to provide a quantitative comparison of the various yield stress reductions reported in the literature. Care must be taken in evaluating this reduction experimentally because the electrical current required to generate a user-specified magnetic flux density may increase at high temperatures. If a fixed current is provided then the actual applied field in the sample may be markedly smaller than assumed, and consequently the measured yield stress will be underestimated.

The thermorheological change in MR yield stress measured in this work is less than the values found in previous literature; however, there remains a fourfold disparity between theoretical expectations (Equation (7)) and the experimental observation (Table 3). One possible explanation for part of this discrepancy may be the effect of temperature on the volume fraction occupied by the ferromagnetic particles in the suspension. Because the hydrocarbon oils used commonly as the suspending medium have higher coefficients of expansion than the particles, during an isobaric increase in temperature the volume fraction occupied by the particles decreases. This change in volume fraction occupied by the particle phase may also lead to a change in the MR yield stress after a sufficient volume of fluid is loaded into the rheometer. The volume fraction of particles at elevated temperature is:

$$\phi_f = \frac{\phi_0\left(1+\alpha_p\Delta T\right)}{1+\phi_0\alpha_p\Delta T+\left(1-\phi_0\right)\alpha_b\Delta T}, \qquad (20)$$

where ϕ_0 is the initial particle volume fraction, and α_b and α_p are the volumetric thermal expansion coefficients for the base fluid and particles respectively. Using this relation we can find the sensitivity of volume fraction to changes in temperature by:

$$S_\phi = \lim_{\Delta T \to 0} \frac{1}{\phi_0} \frac{\phi_f - \phi_0}{\Delta T} = (1-\phi_0)(\alpha_p - \alpha_f). \qquad (21)$$

Typical coefficients of volumetric expansion are $6.3\times10^{-4}/°C$ for mineral oils (Khonsari and Booser, 2001) and $3.54\times10^{-5}/°C$ for iron (calculated from the coefficient of linear expansion given by Lide (2009)). For a fluid with 32% volume fraction, the normalized thermal sensitivity is $-4.0\times10^{-4}/°C$. Because of the linear relationship between volume fraction and yield stress described by Equation (4), this sensitivity is equal to the sensitivity of yield stress caused solely by volumetric expansion effects. However, as noted in the discussion following Equation (4), the linear variation in yield stress with volume fraction is limited to $\phi \lesssim 0.3$ and the equality between the sensitivities is strictly applicable only in this regime. Nevertheless, it is clear that the effect of changes in the effective volume fraction of the magnetic particles with increases in temperature can be important in high-temperature performance of MR fluids.

The shear rheology of a representative commercial MR fluid was characterized over a range of temperatures typical of oilfield applications. The evolution of the MR yield stress was evaluated in terms of the thermal variations in the physical properties of the suspension such as saturation magnetization and volume fraction. Thermal and magnetization shift factors were utilized to collapse the rheological measurements to a reduced MR stress. It is clear from the master curve (Figure 13) that at high fields the reduced stress τ_r is approximately constant with a reference yield stress value of $\tau_y^0 \simeq 11kPa$. Once this material specific reference value is known, the MR stress at a given set of experimental conditions (temperature and magnetic field) can be determined by

$$\tau(T,M) = \tau_y^0 a_Y a_M$$
$$= \tau_y^0 \left(1 + \langle S_\tau \rangle \Delta T\right)\left(\frac{M}{M_0}\right)^\alpha \qquad (22)$$

where M_0 is the reference magnetization corresponding to the magnetic field strength at this reference stress. The magnetic data required to utilize this equation can be determined by performing magnetization measurements on the fluid. In the present study this was taken from the fluid manufacturer's specifications (Lord, 2008). It is also possible to make use of Figure 11 to obtain this data, since each rheological data point is plotted against both the magnetic field strength H and the magnetization M. With the knowledge of the magnetic constitutive relationship of the material $(B = \mu_o(H + M))$, the magnetization shift factor a_M can be calculated as a function of field strength H. In the present study the reference magnetization $M_0 = 1.96 \times 10^5\ A/m$ at $B = 0.3T$ was selected and the power law index was determined to be $\alpha = 1.46 \pm 0.07$. To determine the shift in the yield stress associated with the changes in temperature (denoted a_Y in Equation (22)), the average thermal sensitivity $\langle S_\tau \rangle$ needs to be determined. This quantity varies with temperature and magnetic field (as presented in Table 3); however, an approximate average value of $\langle S_\tau \rangle \approx -9 \times 10^{-4}/°C$ may be useful in the absence of rheological measurements at elevated temperatures. Using these shift factors, it was possible to collapse all of our rheological measurements spanning a temperature range of $20°C - 130°C$ and a magnetic flux density range of $0.3T - 0.9T$ as shown in Figure 13.

Elevated temperatures commonly occur in the operation of MR fluids partly because of the internal heating of the fluid and partly because of the environmental conditions. The results presented here are given in terms of a rheological master curve that is valid at both high fluxes and high temperatures. The experimentally-determined shift factors enable design

calculations incorporating the effects of variation in the magnetic flux and the temperature, and therefore can be used in future developments of MR fluids for extreme temperature applications with the goals of predicting the thermal sensitivity of overall device performance.

Appendix

Magnetic fluid migration

It was observed experimentally that under sufficiently large magnetic field, the high magnetic permeability MR fluid samples fracture and escape from the parallel plate geometry. In this appendix an approximate analysis is presented for calculating the field strength causing this fracture.

The radial components of the Korteweg-Helmholtz stress tensor (Melcher, 1981) are:

$$\begin{aligned} T_{rr} &= \frac{\mu}{2}\left(H_r^{\,2} - H_\theta^{\,2} - H_z^{\,2}\right) \\ T_{r\theta} &= \mu H_r H_\theta \\ T_{rz} &= \mu H_r H_z \end{aligned} \qquad (23)$$

where H_r, H_θ and H_z are the magnetic field strength in the radial, azimuthal and axial directions. We will approximate the sample as a cylindrical disk; treating the ideal case in which the magnetic field is in the z-direction and the material is in the linear magnetization regime. In this case the magnetic pressure jump across the sample perimeter is:

$$\left[\left|T_{rj}.n_j\right|\right] = \frac{\left(\mu_{MRF} - \mu_0\right)}{2} H_z^{\,2} \qquad (24)$$

where μ_{MRF} is the magnetic permeability of MR fluid and n_j is the unit vector with $j = r, \theta, z$ and summation is implied over the repeated indices.. This pressure jump is

balanced only by the one caused by surface tension $p_{st} \sim \sigma/h$ (for a liquid with contact angle $\sim 90°$) where σ is the surface tension (Tanner and Keentok, 1983). Taking typical values for the physical parameters ($\sigma = 0.03N/m$, $\mu_{MRF} = 9\mu_0$ and $h = 0.5mm$) we can find the fracture field $H_z = 3.5kA/m$, which is in agreement with the observed fracture events in the magnetorheometry accessory described in the current study.

It can be seen from this analysis that the magnetic fluids tend to vacate the geometry space and the driving force behind this migration scales with the discontinuity in magnetic permeability.

Acknowledgements

We would like to thank Raoul Smith and Russell Ulbrich of TA Instruments for helpful discussions during design and testing of the magnetorheology accessory, and for providing a notched upper plate geometry. We also thank Prof. Daniel Klingenberg for helpful suggestions and in particular for suggesting the change in volume fraction of MR fluids with temperature.

References

Agarwal BD, Broutman LJ, Chandrashekhara K (2006) Analysis and Performance of Fiber Composites. John Wiley, Hoboken, N.J.

Avallone EA, Baumeister III T (1996) Marks' Standard Handbook for Mechanical Engineers. McGraw-Hill, New York

Barnes HA (1995) A review of the slip (wall depletion) of polymer solutions, emulsions and particle suspensions in viscometers: its cause, character, and cure. J Non-Newton Fluid 56: 221-251

Batterbee DC, Sims ND (2008) Temperature sensitive stability of feedback controllers for MR dampers. SPIE Conference on Active and Passive Smart Structures and Integrated Systems, San Diego, CA, Mar 10-13, 2008. 6928: B9281

Bertola V, Bertrand F, Tabuteau H, Bonn D, Coussot P (2003) Wall slip and yielding in pasty materials. J Rheol 47: 1211-1226. DOI 10.1122/1.1595098

Bhavsar R, Vaidya N, Ganguly P, Humphreys A, Robisson A, Tu H, Wicks N, McKinley GH, Pauchet F (2008) Intelligence in Novel Materials. Oilfield Review 20: 32-41

Bird RB, Armstrong RC, Hassager O (1987) Dynamics of Polymeric Liquids: Volume 1 Fluid Mechanics. Wiley, New York

Blundell S (2001) Magnetism in Condensed Matter. Oxford University Press, Oxford ; New York

Bossis G, Lemaire E, Volkova O, Clercx H (1997) Yield stress in magnetorheological and electrorheological fluids: A comparison between microscopic and macroscopic structural models. J Rheol 41: 687-704

Climent E, Maxey MR, Karniadakis GE (2004) Dynamics of self-assembled chaining in magnetorheological fluids. Langmuir 20: 507-513. DOI 10.1021/la035540z

Cobern ME, Perry CA, Barbely JA, Burgess DE, Wassell ME (2007) Drilling tests of an active vibration damper. SPE/IADC Drilling Conference, 1: 339-348

Crangle J, Goodman GM (1971) Magnetization of pure iron and nickel. P Roy Soc Lond A Mat 321: 477-491

de Vicente J, Klingenberg DJ, Hidalgo-Alvarez R (2011) Magnetorheological fluids: a review. Soft Matter 7: 3701-3710. DOI 10.1039/c0sm01221a

Deshmukh SS (2007) Development, characterization and applications of magnetorheological fluid based 'smart' materials on the macro-to-micro scale. PhD Thesis, Massachusetts Institute of Technology, Dept. of Mech. Eng.

Deshmukh SS, McKinley GH (2004) Rheological Behavior of Magnetorheological Suspensions under Shear, Creep and Large Amplitude Oscillatory Shear (LAOS) Flow. XIVth Int Congr on Rheology, Seoul, Korea, August 22-27, 2004.

Ewoldt RH, Winter P, Maxey J, McKinley GH (2010) Large amplitude oscillatory shear of pseudoplastic and elastoviscoplastic materials. Rheol Acta 49: 191-212. DOI 10.1007/s00397-009-0403-7

Felt DW, Hagenbuchle M, Liu J, Richard J (1996) Rheology of a magnetorheological fluid. J Intel Mat Syst Str 7: 589-593

Fermigier M, Gast AP (1992) Structure evolution in a paramagnetic latex suspension. J Colloid Interf Sci 154: 522-539

Gabriel C, Laun HM (2009) Combined slit and plate-plate magnetorheometry of a magnetorheological fluid (MRF) and parameterization using the Casson model. Rheol Acta 48: 755-768. DOI 10.1007/s00397-009-0369-5

Genc S, Phule PP (2002) Rheological properties of magnetorheological fluids. Smart Mater Struct 11: 140-146

Ginder JM, Davis LC, Elie LD (1996) Rheology of magnetorheological fluids: Models and measurements. Int J Mod Phys B 10: 3293-3303

Halsey TC, Toor W (1990) Structure of electrorheological fluids. Phys Rev Lett 65: 2820-2823

Horvath AT, Klingenberg DJ, Shkel YM (2002) Determination of rheological and magnetic properties for magnetorheological composites via shear magnetization measurements. Int J Mod Phys B 16: 2690-2696

Ida N, Bastos J (1997) Electromagnetics and calculation of fields. Springer, New York

Jackson JD (1999) Classical Electrodynamics. Wiley, New York

Jiles D (1991) Introduction to Magnetism and Magnetic Materials. Chapman and Hall, London ; New York

Jolly MR, Bender JW, Carlson JD (1998) Properties and applications of commercial magnetorheological fluids. In: Davis LP (ed) Passive Damping and Isolation - Smart Structures and Materials 1998, vol 3327, 262-275

Kavlicoglu B, Gordaninejad F, Evrensel C, Fuchs A, Korol G (2006) A semi-active, high-torque, magnetorheological fluid limited slip differential clutch. J Vib Acoust 128: 604-610. DOI 10.1115/1.2203308

Khonsari MM, Booser ER (2001) Applied Tribology : Bearing Design and Lubrication. John Wiley, New York

Klingenberg DJ (2001) Magnetorheology: Applications and challenges. AIChE Journal 47: 246-249

Klingenberg DJ, Ulicny JC, Golden MA (2007) Mason numbers for magnetorheology. J Rheol 51: 883-893. DOI 10.1122/1.2764089

Klingenberg DJ, Vanswol F, Zukoski CF (1991) The small shear rate response of electrorheological suspensions 1. Simulation in the point-dipole limit. J Chem Phys 94: 6160-6169

Klingenberg DJ, Zukoski CF (1990) Studies on the steady-shear behavior of electrorheological suspensions. Langmuir 6: 15-24

Kordonski W, Shorey A (2007) Magnetorheological (MR) jet finishing technology. J Intel Mat Syst Str 18: 1127-1130. DOI 10.1177/1045389x07083139

Kuzhir P, Bossis G, Bashtovoi V (2003a) Effect of the orientation of the magnetic field on the flow of a magnetorheological fluid. I. Plane channel. J Rheol 47: 1373-1384. DOI 10.1122/1.1619377

Kuzhir P, Bossis G, Bashtovoi V, Volkova O (2003b) Effect of the orientation of the magnetic field on the flow of magnetorheological fluid. II. Cylindrical channel. J Rheol 47: 1385-1398. DOI 10.1122/1.1619378

Kuzhir P, Lopez-Lopez MT, Bossis G (2009) Abrupt contraction flow of magnetorheological fluids. Phys Fluids 21: 053101. DOI 10.1063/1.3125947

Laeuger J, Wollny K, Stettin H, Huck S (2005) New device for the full rheological characterization of magneto-rheological fluids. Int J Mod Phys B 19: 1353-1359
Laun HM, Gabriel C (2007) Measurement modes of the response time of a magneto-rheological fluid (MRF) for changing magnetic flux density. Rheol Acta 46: 665-676. DOI 10.1007/s00397-006-0155-6
Laun HM, Gabriel C, Kieburg C (2010) Twin gap magnetorheometer using ferromagnetic steel plates-Performance and validation. J Rheol 54: 327-354. DOI 10.1122/1.3302804
Laun HM, Gabriel C, Kieburg C (2011) Wall material and roughness effects on transmittable shear stresses of magnetorheological fluids in plate-plate magnetorheometry. Rheol Acta 50: 141-157. DOI 10.1007/s00397-011-0531-8
Laun HM, Gabriel C, Schmidt G (2008a) Primary and secondary normal stress differences of a magnetorheological fluid (MRF) up to magnetic flux densities of 1 T. J Non-Newton Fluid 148: 47-56. DOI 10.1016/j.jnnfm.2007.04.019
Laun HM, Kormann C, Willenbacher N (1996) Rheometry on magnetorheological (MR) fluids .1. Steady shear flow in stationary magnetic fields. Rheol Acta 35: 417-432
Laun HM, Schmidt G, Gabriel C, Kieburg C (2008b) Reliable plate-plate MRF magnetorheometry based on validated radial magnetic flux density profile simulations. Rheol Acta 47: 1049-1059. DOI 10.1007/s00397-008-0305-0
Li WH, Chen G, Yeo SH (1999) Viscoelastic properties of MR fluids. Smart Mater Struct 8: 460-468
Li WH, Chen G, Yeo SH, Du H (2002) Temperature dependence of MR fluids. Int J Mod Phys B 16: 2725-2731
Lide DR, ed. (2009) CRC Handbook of Chemistry and Physics, 89th Edition (Internet Version). CRC Press/Taylor and Francis, 12/203
Lord (2008) MRF-132DG magneto-rheological fluid technical data sheet, http://www.lordfulfillment.com/upload/DS7015.pdf. Accessed March 14, 2008
Macosko CW (1994) Rheology : Principles, Measurements, and Applications. VCH, New York
Marshall L, Zukoski CF, Goodwin JW (1989) Effects of electric-fields on the rheology of non-aqueous concentrated suspensions. J Chem Soc Farad T 1 85: 2785-2795
Melcher JR (1981) Continuum Electromechanics. MIT Press
Mills AF (1999) Heat Transfer. Prentice Hall; Prentice-Hall International (U.K.), Upper Saddle River, N.J. London
Ocalan M, McKinley GH (2012) Rheology and microstructural evolution in pressure-driven flow of a magnetorheological fluid with strong particle-wall interactions. J Intel Mat Syst Str 23: 969-978
Park JH, Chin BD, Park OO (2001) Rheological properties and stabilization of magnetorheological fluids in a water-in-oil emulsion. J Colloid Interf Sci 240: 349-354
Ponticel P (2002) New magnetorheological fluids from LordAutomotive Engineering International Online. SAE International, http://www.sae.org/automag/material/08-2002/. Accessed November 1, 2009
Promislow JHE, Gast AP, Fermigier M (1995) Aggregation kinetics of paramagnetic colloidal particles. J Chem Phys 102: 5492-5498
Rabinow J (1948) The magnetic fluid clutch. Trans Am Inst Electr Eng 67: 1308-1315
Rankin PJ, Horvath AT, Klingenberg DJ (1999) Magnetorheology in viscoplastic media. Rheol Acta 38: 471-477
Sahin H, Wang XJ, Gordaninejad F (2009) Temperature Dependence of Magneto-rheological Materials. J Intel Mat Syst Str 20: 2215-2222. DOI 10.1177/1045389x09351608
Serway RA (1990) Physics for Scientists & Engineers, with Modern Physics. Saunders College Pub., Philadelphia
Shkel YM, Klingenberg DJ (2001) Magnetorheology and magnetostriction of isolated chains of nonlinear magnetizable spheres. J Rheol 45: 351-368
Shul'man ZP, Kordonskii VI, Prokhorov IV (1980) Magnetorheological effect near the Curie point. J Eng Phys 38: 79-80
Stedfeld RL, Zorc TB (1995) ASM Handbook, Volume 2, Properties and Selection: Nonferrous Alloys and Special-Purpose Materials. ASM International
Stickel JJ, Powell RL (2005) Fluid mechanics and rheology of dense suspensions. Annu Rev Fluid Mech 37: 129-149. DOI 10.1146/annurev.fluid.36.050802.122132
Tanner RI, Keentok M (1983) Shear fracture in cone-plate rheometry. J Rheol 27: 47-57
Tao R (2001) Super-strong magnetorheological fluids. J Phys-Condens Mat 13: R979-R999
Ulicny JC, Golden MA, Namuduri CS, Klingenberg DJ (2005) Transient response of magnetorheological fluids: Shear flow between concentric cylinders. J Rheol 49: 87-104. DOI 10.1122/1.1803576
Wang XJ, Gordaninejad F (2006) Study of magnetorheological fluids at high shear rates. Rheol Acta 45: 899-908. DOI 10.1007/s00397-005-0058-y
Weiss KD, Carlson JD, Nixon DA (1994) Viscoelastic properties of magnetorheological and electrorheological fluids. J Intel Mat Syst Str 5: 772-775

Woodson HH, Melcher JR (1968) Electromechanical Dynamics. Wiley, New York,
Zahn M (1987) Electromagnetic Field Theory : A Problem Solving Approach. R.F. Krieger, Malabar, Fla.
Zschunke F, Rivas R, Brunn PO (2005) Temperature behavior of magnetorheological fluids. Appl Rheol 15: 116-121

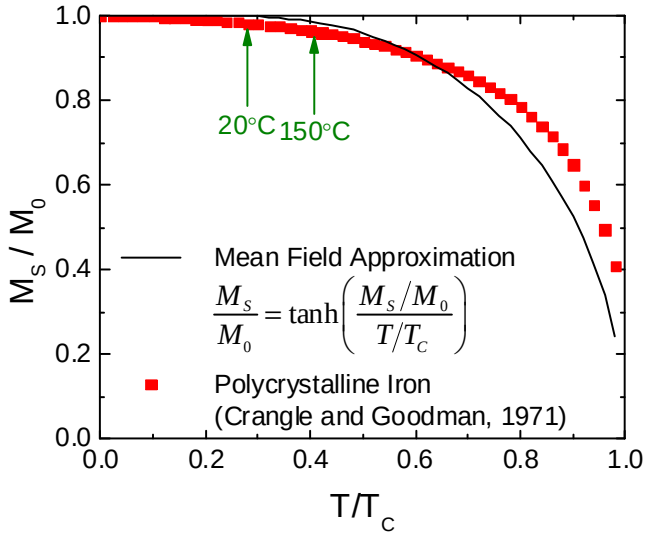

Fig. 1: Evolution of saturation magnetization of polycrystalline iron with temperature. The locations corresponding to $20°C\left(T/T_C = 0.28\right)$ and $150°C\left(T/T_C = 0.41\right)$ are marked to provide a quick reference.

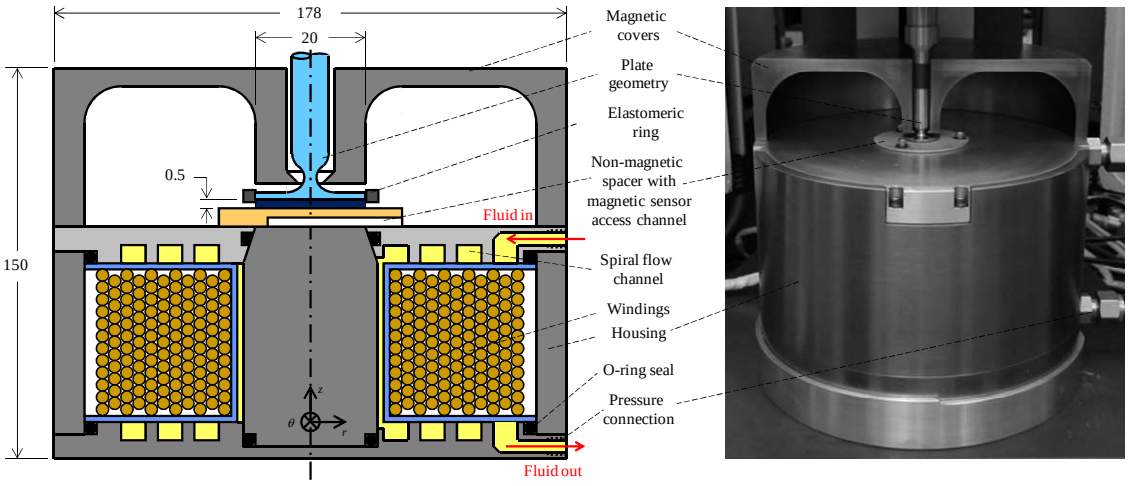

(a) (b)

Fig. 2: (a) Schematic diagram and (b) photograph of magnetorheometry fixture. Dimensions are given in mm.

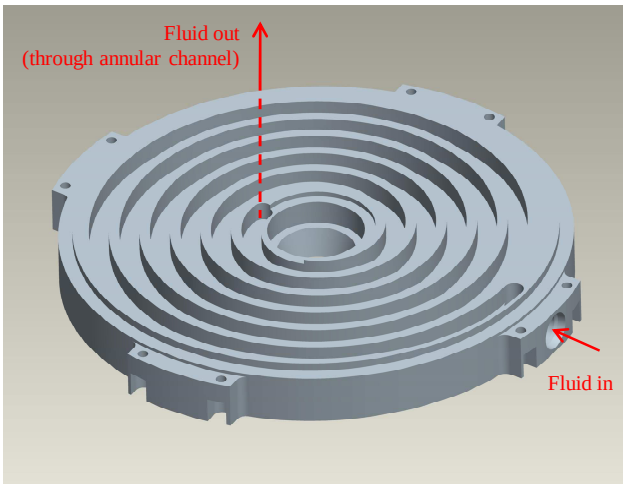

Fig. 3: Model of the central plate. A spiral flow channel is machined onto the plate. A similar flow channel is machined on the lower magnetic plate. These two channels are linked with the annular flow path between the magnetic core and the bobbin.

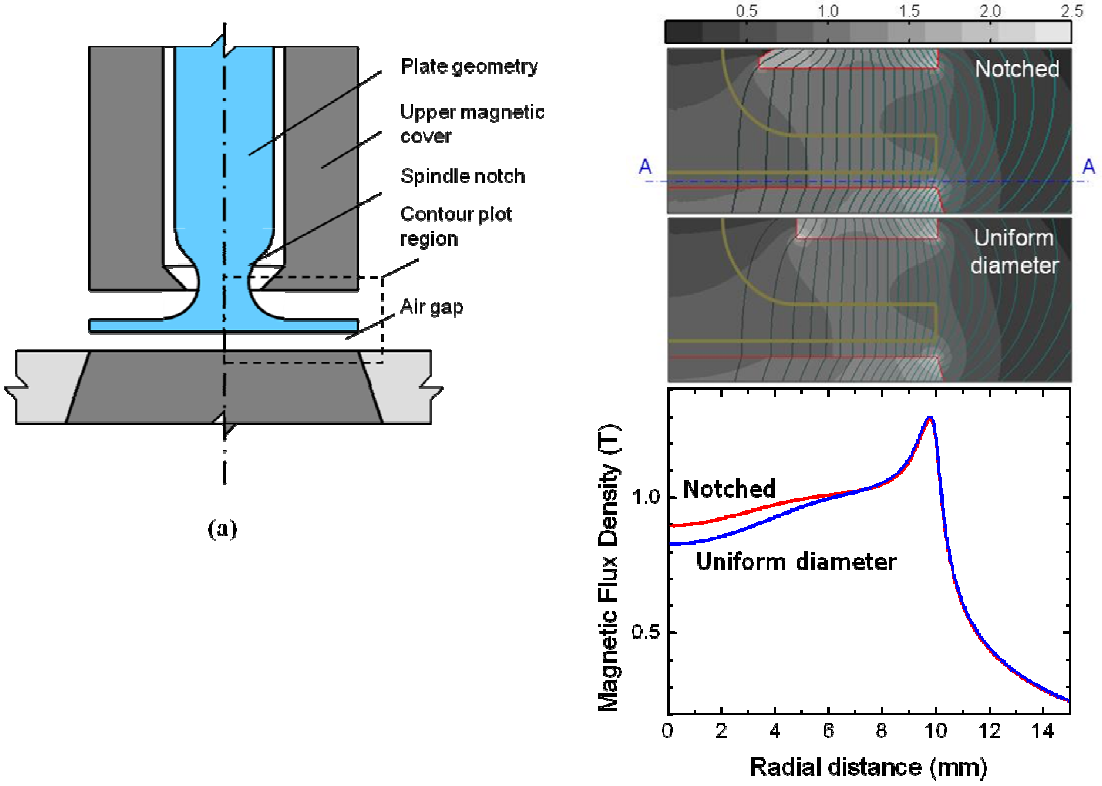

Fig. 4: Design of the upper plate geometry and the magnetic covers. Reducing the access hole diameter for the rheometer spindle near the sample increases field uniformity. a) Schematic diagram of the gap region. b) Contour plot of magnetic flux density and flux lines in the air gap for a notched and uniform diameter spindle. The coil current in the simulation is 5A. The line plots are drawn at the axial location of $z = 250\mu m$ (denoted by line AA) above the lower magnetic core (i.e. at the mid-span of a typical sample height, $h = 500\mu m$)

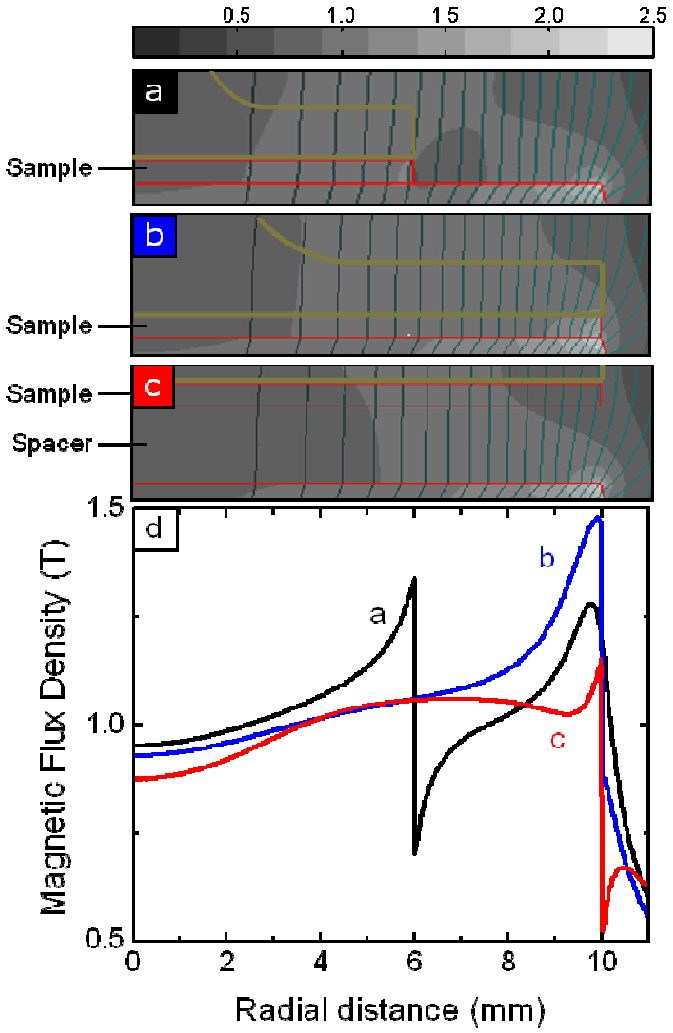

Fig. 5: Magnetic flux density and flux line contours for a) 12mm diameter sample, b) 20mm diameter sample placed directly on magnetic core and c) 20mm diameter sample on 1.6mm thick non-magnetic spacer; d) Line plots of magnetic flux density along radius at the axial mid-plane of $h = 500\mu m$.

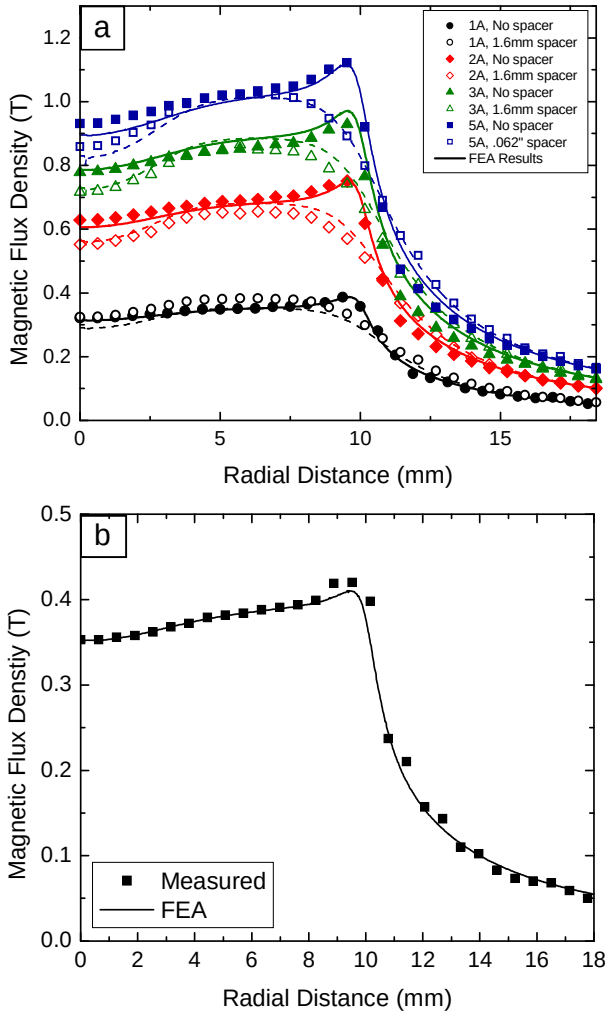

Fig. 6: Finite element results compared with experimental measurements for a range of currents $(1A \le I \le 5A)$ for sample gap $(h = 0.5mm)$ filled with a) air and b) MR fluid (Lord MRF-132DG). The finite element results are plotted along the radius of the MR fixture on the plane of the Hall Effect sensor ($z = 572\mu m$) to provide the most representative comparison. The uniformity in the magnetic field is improved by the non-magnetic spacer used directly beneath the MR fluid sample.

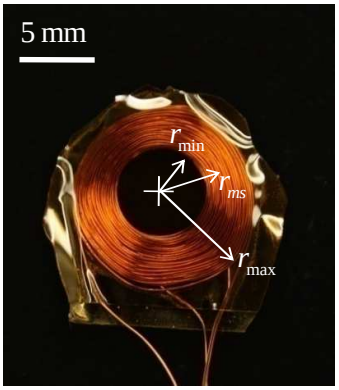

Fig. 7: Photograph of secondary (sensing) coil. This coil was used in the elevated temperature experiments to measure field strength ($r_{min} = 3.2mm$, $r_{max} = 8.0mm$).

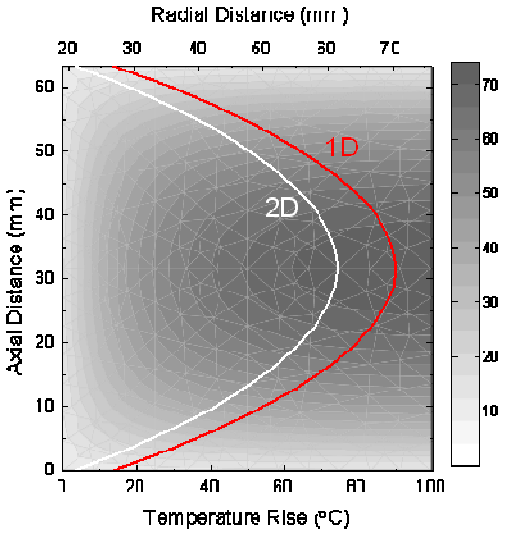

Fig. 8: Axial distribution of temperature rise for (i) 1D analytical model in red and (ii) insulated outer wall of 2D numerical model (blue). Background is the contour plot of the expected temperature rise obtained from the numerical model. The contour bar shows temperature rise in $°C$ corresponding to $q''' = 1.2\times10^5\, W/m^3$ and $Bi = 45$.

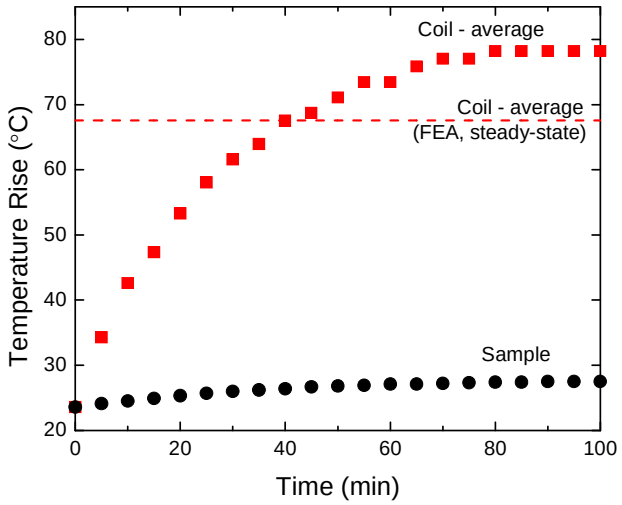

Fig. 9: Evolution of sample chamber temperature and average coil temperature after a step increase in the current input of $\Delta I = 5A$ at t = 0. Data is recorded until steady-state is reached. The coil temperature climbs $\Delta T = 55°C$; however this results in a change of only $4°C$ in sample temperature. The average coil temperature is calculated from the change measured in the electrical resistance of the winding using Equation (13).

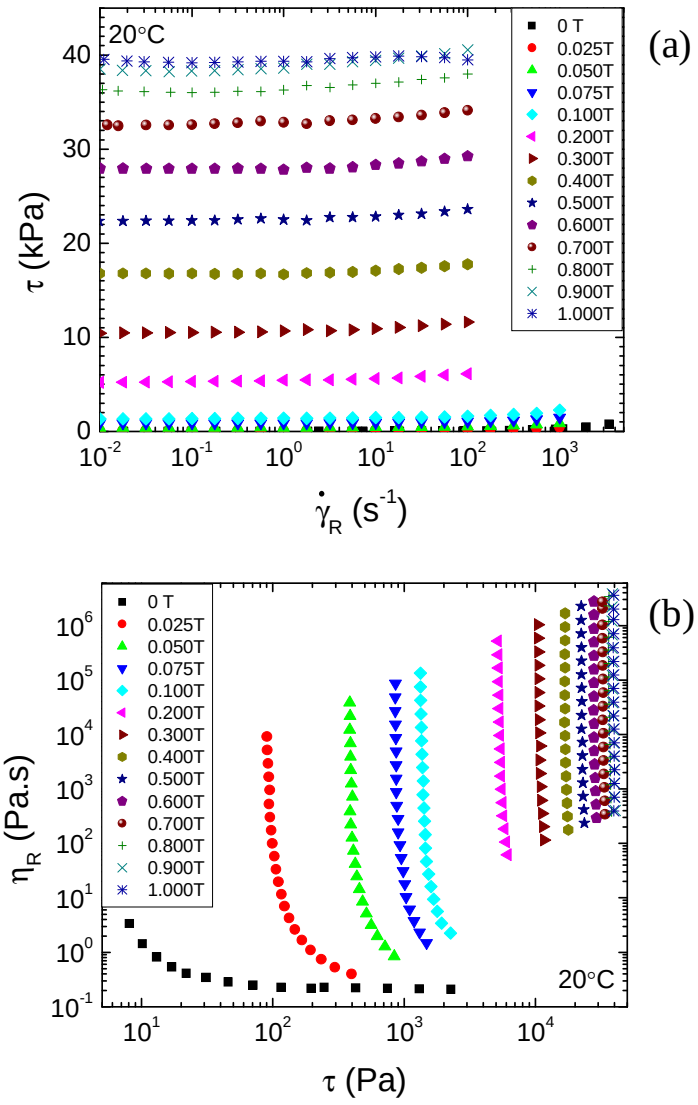

Fig. 10: Experimental results for rate-controlled steady shear viscosity of a magnetorheological fluid (Lord® MRF-132DG). (a) Semilogarithmic plot of the measured shear stress showing that it is essentially flat over four orders of magnitude increase in the shear rate. The fluid rheology is dominated by the field-dependent yield stress $\tau_y(B)$. (a) The dynamic yield stress values for each magnetic field point can be easily seen in the vertical asymptotes of the viscosity vs. shear stress plot. There is a small yield stress also present in the field-off data however this is very weak compared to field-on yield stress ($\tau_y^{off} < 5Pa$). In the limit of high shear rates the field-on plots tend towards the field-off viscosity as the viscous stress acting on the suspended particles becomes the same order of magnitude as the magnetic stress ($Mn \sim 1$).

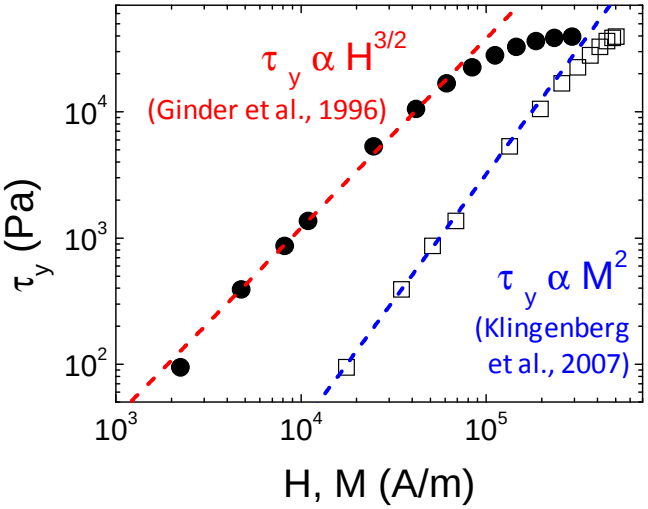

Fig. 11: Evolution of MR yield stress with magnetic field strength *H*, and magnetization, *M*. At lower field strengths the asymptotic scaling laws identified by Ginder and coworkers (1996), and Klingenberg and coworkers (2007) accurately describe the evolution of MR fluid rheology. At higher fields $(B > 0.3T)$, however, there is significant deviation of experimental results from each of the scaling laws.

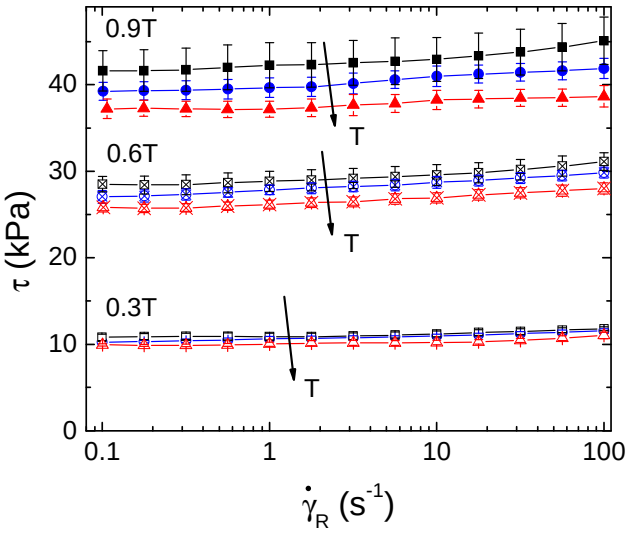

Fig. 12: Evolution in magnetorheological shear stress with increasing temperature. Black squares, blue circles and red triangles are data at T = 20°C, T = 75°C and T = 130°C respectively. Five samples measured at each temperature and magnetic field level. Bars designate the standard deviation $\pm\sigma$. There is a systematic and statistically significant decrease in the yield stress with temperature which becomes larger at high temperatures and high field strengths. The sensitivity $S_\tau(T)$ is tabulated in Table 3.

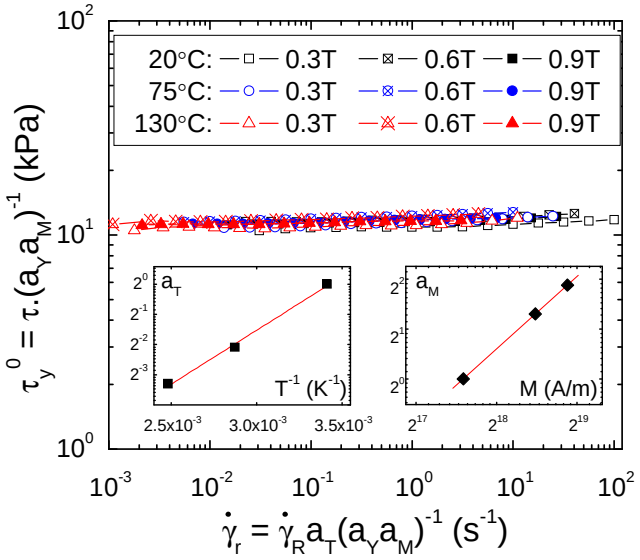

Fig. 13: Magnetorheological measurements shifted with the magnetic shift factor, a_M, the thermoviscous shift factor, $a_T = \eta_\infty(T)/\eta_\infty(T_0)$ and the MR stress thermal shift factor a_Y. In the subplot on the left, the line indicates the function $a_T = \exp\left[2470K\left(1/T - 1/291K\right)\right]$ found by curve fitting to the values of a_T found at each temperature. The line in the right subplot shows the fitted function $a_M = \left(M/M_0\right)^{1.46}$. Using these factors, the measurements made across the magnetic field and temperature ranges studied can be collapsed onto a single curve. The success of the collapse indicates that the magnetorheological stress scales sub-quadratically with magnetization, *M*, with a power law index of 1.46 ± 0.07.